 CMES, vol.64, no.2, pp.187-212, 2010

# Numerical Solution of Non-Isothermal Fluid Flows Using Local Radial Basis Functions (LRBF) Interpolation and a Velocity-Correction Method

**G. C. Bourantas[1], E. D. Skouras[2,3], V. C. Loukopoulos[4]**
**G. C. Nikiforidis[1]**

**Abstract:** Meshfree point collocation method (MPCM) is developed, solving the velocity-vorticity formulation of Navier-Stokes equations, for two-dimensional, steady state incompressible viscous flow problems in the presence of heat transfer. Particular emphasis is placed on the application of the velocity-correction method, ensuring the continuity equation. The Gaussian Radial Basis Functions (GRBF) interpolation is employed to construct the shape functions in conjunction with the framework of the point collocation method. The cases of forced, natural and mixed convection in a 2D rectangular enclosure are examined. The accuracy and the stability of the proposed scheme are demonstrated through three representative, well known and established benchmark problems. Results are presented for high values of the characteristics non-dimensional numbers of the flow, that is, the Reynolds, the Rayleigh and the Richardson number.

**Keywords:** Meshfree point collocation method, LRBF, Velocity-vorticity formulation, 2D incompressible Navier-Stokes equations, Velocity-correction method.

## 1 Introduction

Many physical problems are modeled with partial differential equations (PDEs). Moreover, a high number of numerical methods and techniques have been developed for the solution of the PDEs and, they are focused mainly on the improvement of accuracy and efficiency of them. In recent years attention has turned on the development of meshless/meshfree methods, especially for the numerical solution of

[1] Department of Medical Physics, School of Medicine, University of Patras, GR 26500, Rion, Greece.
[2] Department of Chemical Engineering, University of Patras, GR 26500, Rion, Greece.
[3] Institute of Chemical Engineering and High Temperature Chemical Processes - Foundation for Research and Technology, P.O. Box 1414, GR-26504, Patras, Rion, Greece.
[4] Department of Physics, University of Patras, Patras, 26500, Rion ,Greece.

partial differential equations. Their key advantage over the traditional mesh/grid based numerical methods, such as Finite Element Method (FEM), Finite Volume Method (FVM) and Finite Difference Method (FDM), is that the computational domain used rely on a particle (either Lagrangian or Eulerian) view of the field problem, eliminating the use of a computational mesh/grid [Liu (2002), Atluri and Shen (2002)]. Thus, functional interpolation or approximation is constructed entirely from the information given by a set of scattered nodes or particles, among which there is no pre-specified connectivity or relationships.

Several meshfree methods have been proposed since the prototype of the meshfree methods, the Smoothed Particle Hydrodynamics (SPH), was born [Belytschko, Krongauz, Organ, Fleming and Krysl (1996)]. Regarding of the meshless methods, according to the formulation procedures they can be classified into two major categories, namely the collocation-based and the Galerkin-based methods, solving the strong- and weak-forms of the problems considered, respectively. Both formulations pose advantages and limitations [Liu (2005)]. Galerkin are difficult to implement, since they rely on a background mesh for the integral evaluation, but stable, while collocation based method are easy to implement, truly meshless, although having less stability. Furthermore, according to the function approximation/interpolation schemes, MFree methods are based on moving least squares (MLS) approximation, on the integral representation method and finally, on the point interpolation method (PIM). Especially for the PIM methods, two different types of formulation have been developed, the first uses the polynomial basis while the second the radial basis functions (RBF).

In the last decade, meshfree methods utilizing radial basis functions have been extensively used. In 1990, Kansa [Kansa (1990)] introduced a technique for solving numerically partial differential equations by collocation method using radial basis functions. In Kansa's approach, the solution is approximated by radial basis functions, and the collocation method is used to compute the unknown coefficients. Thereafter, several radial basis functions were introduced, using different forms of radial functions. Kansa's method has been further upgraded to symmetric collocation [Fasshauer (1997), Power and Barraco (2002)], to modified collocation [Chen (2002)], and to indirect collocation [Mai-Duy and Tran-Cong (2003)]. Unfortunately, all of the above listed methods usually fail to perform on large problems, since they produce fully populated matrices, which are sensitive to the choice of the free parameters in RBFs. Thus, these methods are impractical for real problems arising in science and engineering.

In order to overcome that limitation, sparse matrices can be generated by the introduction of the compactly supported RBFs. Furthermore, the accuracy of such an approach can be improved further by the multilevel technique [Chen, Ganesh,

Golberg and Cheng (2002)]. One of the possibilities for mitigating the large fully-populated matrix problem is to employ domain decomposition procedures [Mai-Duy and Tran-Cong (2002)]. However, the domain decomposition reintroduces some sort of meshing, which is not generally attractive. Thus, the concept of local collocation in the context of an RBF-based solution has been introduced. By using the local RBFs the only geometrical data needed for the construction of the matrices are for those nodes that fall into the influence domain of each node. Moreover, the properties of the constructed shape functions are the same with those for the global RBF, and the approximation method is stable and insensitive to the free parameter needed for the formulation. Additionally, the computational cost is decreasing since the matrix operations require the inversion of matrices of small size, equal to the number of nodes in the support domain [Lee, Liu and Fan (2003)]. It can be seen that the local RBF collocation approach differs of the classical global RBF collocation approach in the way that a radial basis function (RBF) interpolation function is defined. The former chooses to represent the meshless approximation by an expansion around a few supporting points (it constitutes a computational molecule). Any Lagrangian or Hermitian RBF Hardy's interpolation can be used to construct the meshless locally-supported shape functions, which can reconstruct the field variable in each point into the molecule. In this way, several strategies have been proposed to possibly improve the imposing of the derivative boundary conditions in a strong-form approach.

The subject of heat transfer is of fundamental importance in many branches of engineering. Knowing the mechanism of heat transfer involved in the operation of equipments such as boilers, condensers, air pre-heaters, economizers, semiconductor devices, electric motors, electric generators and others, engineers can improve their performance. Due to its importance, numerous works are dealing with the physical problem mentioned above, using a variety of meshless schemes. More precisely, in [Mai-Duy and Tran-Cong (2001)] authors used the Indirect Radial Basis Function Networks (IRBFN) along with the point collocation method and solved the laminar, incompressible Navier-Stokes equations in streamfunction–vorticity formulation for the lid-driven cavity with natural convection benchmark problem up to Rayleigh number $Ra = 10^6$, using a relatively coarse grid of $61 \times 61$ regular distributed nodes. In [Wu and Liu (2003)] a square enclosure, along with a concentric annulus, two-dimensional natural convection problems were investigated. The Local Radial Interpolation Method (LRPIM) was adopted in order to simulate the fluid flow problem. The vorticity-stream function form of Navier-Stokes equations was taken as the governing equation. The Rayleigh numbers used were in the range of $10^3 \leq Ra \leq 10^5$. Conjugate heat transfer problems modeled by convecting fully viscous incompressible fluid interacting with conducting solids were considered in

[Divo and Kassab (2006)]. Therein, the meshless formulation for fluid flow modeling is based on a radial basis function interpolation using inverse Multiquadrics and a time-progression decoupling of the equations using a Helmholtz potential. For the lid-driven cavity Reynolds number $Re = 400$ was used for. The same authors [Divo and Kassab (2007), Divo and Kassab (2008)] developed the RBF-based localized collocation meshless method (LCMM) where the fully coupled incompressible Navier–Stokes equations are solved in strong form. Furthermore, a local radial basic function based gridfree scheme has been developed to solve the unsteady, incompressible heat transfer and fluid flow problems [Sarler (2005)]. In continuation, specifics of a primitive variable solution procedure for the coupled mass, momentum, and energy transport representing the natural convection in an incompressible Newtonian Bussinesq fluid are elaborated. Collocation strategy is performed with Prandtl number $Pr = 0.71$ and Rayleigh numbers $Ra = 10^3 - 10^6$. Authors in [Kosec and Sarler (2008)] solved the pressure-velocity formulation of the Navier-Stokes and thermal equations for natural convection flow. Using multiquadric radial basis functions obtained numerical results for Rayleigh number up to $10^8$. Therein, authors used a pressure-correction technique and they proposed a much simplified local pressure-velocity coupling (LPCV) algorithm , instead of solving the pressure Poisson equation. Furthermore, authors in [Sarler, Perko and Chen (2004), Sarler and Vertnik (2006)] developed the RBF collocation method for the Darcy flow in porous media as well as natural convection problems by solving the governing equations in strong form over localized data center stencils. The Meshless Local Petrov-Galerkin method (MLPG) was utilized for solving non-isothermal fluid flow problems [Arefmanesh, Najafi and Abdi (2008)]. The Navier-Stokes equations in terms of the stream function and vorticity formulation, together with the energy equation were solved, considering a non-isothermal lid-driven cavity flow, a lid-driven cavity flow with an inlet and outlet, and also a non-isothermal flow over an obstacle. Results were obtained for Reynolds number up to $Re = 400$. Authors in [Ho-Minh, Mai-Duy and Tran-Cong (2009)] reported a new discretization technique for the streamfunction-vorticity-temperature $(\psi - \omega - T)$ formulation governing natural convection defined in 2D enclosured domain. Two benchmark test problems, namely free convection in a square slot and a concentric annulus, were considered. A convergent solution for the former was achieved up to the Rayleigh number of $Ra = 10^8$ with a relatively coarse grid of $51 \times 51$ nodal distribution. Numerical results of natural convection flows in two-dimensional cavities, filled with air, are presented to study the effects on the characteristics of the flows as some parameters vary namely, the Rayleigh number $Ra$ and the aspect ratio $A$ of the cavity. The steady state problem was considered for $10^5 \leq Ra \leq 10^7$ and $\frac{1}{4} \leq A \leq 4$.

Herein, we utilize the velocity-vorticity formulation of Navier-Stokes equations along with the velocity-correction scheme in order to solve forced, natural and mixed convection flow in a rectangular enclosure. The application of velocity-correction method, ensuring the continuity equation permits us to attain solutions for high values of characteristic non-dimensional numbers of the flow. The paper is presented as follows. In Section 2, the Local Radial Basis Functions (LRBFs) interpolation is briefly introduced. The velocity-vorticity formulation based on the meshfree point collocation method is next briefly developed in Section 3 where the implementations of the vorticity boundary conditions are emphasized. In Section 4, several numerical examples of steady-state flow are presented, which demonstrate the performance of the method. Finally, conclusion and discussion complete the paper.

## 2 Basic Concepts of Meshfree Techniques

In the localized collocation meshless methods (LCMM), spatial discretization is performed over uniformly or non-uniformly distributed points, called nodes. Each node is influenced by a set of neighboring points, defining a local topology of surrounding nodes, namely the support domain. The LCMM can handle both the radial basis function collocation and the polynomial expansion with MLS treatment. Herein, attention will be focused on the local radial basis function formulation.

### *2.1 Defining the support domain*

Each point at the interior domain and on the boundaries of the discretized geometry is identified as a data center that uses a set of neighboring influence points to define a localized interpolation topology. At this new defined topology of points the field variable or variables are estimated using the proper functions. For the LCMM considered in this paper, those functions consist of Radial Basis Functions. The total number of points in the support domain, including the data center and the neighboring influence points, is denoted by $N_F$. The definition of the support domain is accomplished by defining a constant number of local neighbors for each data center. The current local topology structure is fixed, that is the number of nodes in the support domains retains constant, however, this structure can be set to change based on the progress of the numerical solution. For example, a modification of the topology size and structure can take place, as long as the numerical solution process is running in order to maintain stability for the solution.

### 2.2 Local Radial Basis Functions

Consider a function $u(\mathbf{x})$ defined in the spatial domain $\Omega$. The domain is represented by a set of nodes scattered (in a uniform or in a non-uniform manner) in the problem domain and on the boundary $\partial\Omega$. The function $u(\mathbf{x})$ is then interpolated using the nodal values at the nodes of the support domain of a point of interest at $\mathbf{x}_Q$. The approximation $u^h(\mathbf{x})$ of a function $u(\mathbf{x})$ at an arbitrary point $\mathbf{x}$ can be written, using the following finite series representation, as:

$$u(\mathbf{x}) \approx u^h(\mathbf{x},\mathbf{x}_Q) = \sum_{i=1}^{n} \Phi_i(\mathbf{x}) a_i(\mathbf{x}_Q), \tag{1}$$

where $\Phi_i(\mathbf{x})$ are the basis functions defined in the Cartesian coordinate space $\mathbf{x}^T = [x,y,z]$, $n$ is the number of nodes in the support domain of point $\mathbf{x}_Q$ and, $a_i(\mathbf{x}_Q)$ is the coefficient for the basis function $\Phi_i(\mathbf{x})$ corresponding to the given point $\mathbf{x}_Q$.

We choose radial functions as the basis in Eq. 2, thus

$$u^h(\mathbf{x},\mathbf{x}_Q) = \sum_{i=1}^{n} R_i(\mathbf{x}) a_i(\mathbf{x}_Q) = R^T(\mathbf{x}) a(\mathbf{x}), \tag{2}$$

where vector $\mathbf{a}$ is defined as $\mathbf{a}^T(\mathbf{x}_Q) = \{a_1, a_2, a_3, ..., a_n\}$ and $R_i$ is a radial basis function with $r$ the distance between point $\mathbf{x}$ and $\mathbf{x}_i$. For a 2D problem, $r$ is defined as $r = \sqrt{(x-x_i)^2 + (y-y_i)^2}$. The vector $\mathbf{R}$ has the form

$$\mathbf{R}^T(\mathbf{x}) = [R_1(\mathbf{x}), R_2(\mathbf{x}), ...., R_n(\mathbf{x})]. \tag{3}$$

There are a number of forms of radial basis functions used by the mathematics community. Table 1 lists the four most often used forms of radial functions with some shape parameters that can be tuned for better performance.

Enforcing $u(\mathbf{x})$ approximated by Eq. 2 to pass through each scattered node in the support domain that is formed for the point of interest $\mathbf{x}$, we have the moment matrix of RBF:

$$\mathbf{R}_Q = \begin{bmatrix} R_1(r_1) & R_2(r_1) & ... & R_n(r_1) \\ R_1(r_2) & R_2(r_2) & ... & R_n(r_2) \\ ... & ... & ... & ... \\ R_1(r_n) & R_2(r_n) & & R_n(r_n) \end{bmatrix}, \tag{4}$$

where

$$r_k = \sqrt{(x_k - x_i)^2 + (y_k - y_i)^2}, \quad k = 1,2,...,n. \tag{5}$$

Table 1: Typical conventional form of Radial Basis Functions.

| ***Item*** | ***Name*** | ***Expression*** | **Shape Parameters** |
|---|---|---|---|
| 1 | Multiquadrics (MQ) | $R_i(x,y) = \left(r_i^2 + C^2\right)^q = \left[(x-x_i)^2 + (y-y_i)^2 + C^2\right]^q$ | $C, q$ |
| 2 | Gaussian (GA) | $R_i(x,y) = e^{-cr_i^2} = e^{-c\left((x-x_i)^2+(y-y_i)^2\right)}$ | $c$ |
| 3 | Thin plate splines (TPS) | $R_i(x,y) = r_i^\eta = \left[(x-x_i)^2 + (y-y_i)^2\right]^\eta$ | $\eta$ |
| 4 | Logarithmic RBF | $R_i(r_i) = r_i^\eta \log r_i$ | $\eta$ |

Since distance is directionless, we should have

$$R_i(r_j) = R_j(r_i). \tag{6}$$

therefore, the moment matrix $R_Q$ is symmetric.

The vectors of coefficients **a** in Eq. 2 are determined by enforcing that the interpolation passes through all the $n$ nodes within the support domain. The interpolation at the $k^{th}$ point has the form:

$$u_k^h = u^h(x_k, y_k) = \sum_{i=1}^{n} a_i R_i(x_k, y_k), \quad k = 1, 2, ..., n, \tag{7}$$

or in matrix form:

$$\mathbf{U}_s = \mathbf{R}_Q \mathbf{a}, \tag{8}$$

where $\mathbf{U}_s$ is the vector that collects all the field nodal variables at the n nodes in the support domain. A unique solution for vectors of coefficients **a** is obtained if the inverse of $\mathbf{R}_Q$ exists:

$$\mathbf{a} = \mathbf{R}_Q^{-1} \mathbf{U}_s. \tag{9}$$

Substituting the foregoing equation into Eq. 2 leads to

$$u^h(\mathbf{x}) = \mathbf{R}^T(\mathbf{x}) \mathbf{R}_Q^{-1} \mathbf{U}_s = \Phi(\mathbf{x}) \mathbf{U}_s, \tag{10}$$

where the matrix of shape functions $\mathbf{\Phi}(\mathbf{x})$ with $n$ shape functions is:

If we define

$$\begin{aligned} \mathbf{\Phi}(\mathbf{x}) &= [R_1(\mathbf{x}), R_2(\mathbf{x}), ..., R_k(\mathbf{x}), ..., R_n(\mathbf{x})] R_Q^{-1} = \\ &= [\phi_1(\mathbf{x}), \phi_2(\mathbf{x}), ..., \phi_k(\mathbf{x}), ..., \phi_n(\mathbf{x})] \end{aligned} \tag{11}$$

in which $\phi_k(\mathbf{x})$ is the shape function for the $k^{th}$ node given by

$$\phi_k(\mathbf{x}) = \sum_{i=1}^{n} R_i(\mathbf{x}) S_{ik}^a, \tag{12}$$

where $S_{ik}^a$ is the $(i,k)$ element of matrix $\mathbf{R}_Q^{-1}$, which is a constant matrix for given locations of the $n$ nodes in the support domain.

The derivatives of shape functions can be easily obtained as

$$\frac{\partial^m \phi_k}{\partial x^m} = \sum_{i=1}^{n} \frac{\partial^m R_i}{\partial x^m} S_{ik}^a, \tag{13}$$

$$\frac{\partial^m \phi_k}{\partial y^m} = \sum_{i=1}^{n} \frac{\partial^m R_i}{\partial y^m} S_{ik}^a, \tag{14}$$

where $m$ is the derivative order, which in our case is $m = 1, 2$.

The Gaussian and the inverse multiquadric, i.e. $q < 0$ in the multiquadric function, are positive definite functions, while the thin-plate splines and the multiquadric, i.e. $q > 0$ in the multiquadric function, are conditionally positive definite functions of order $q$, which require the addition of a polynomial term $P$ of order $q-1$ together with some homogeneous constraint conditions in order to obtain an invertible interpolation matrix $\mathbf{R}_Q$ [Fasshauer (2007), Power and Barraco (2002)]. Since, we have not used that polynomial term, all the computations obtained, took place using the Gaussian form of radial basis functions.

## 3 Governing equations and solution procedure

### *3.1 Governing equations*

The flow and heat transfer phenomena considered herein are described by the complete Navier-Stokes and energy equations for two dimensional laminar incompressible flows. Within the framework of the Cartesian coordinate system, the steady Navier-Stokes equations are expressed in dimensional form as:

*Continuity equation*

$$\nabla \cdot \mathbf{u}^* = 0. \tag{15}$$

*Momentum equation*

$$(\mathbf{u}^* \cdot \nabla)\, \mathbf{u}^* = \mathbf{g} - \frac{1}{\rho_f} \nabla p^* + \frac{\mu_f}{\rho_f} \nabla^2 \mathbf{u}^* + \mathbf{F}. \tag{16}$$

*Energy equation*

$$(\mathbf{u}^* \cdot \nabla)\, T^* = \alpha_f \nabla^2 T^*. \tag{17}$$

where $\mathbf{u}^*$ is the dimensional velocity, $p$ is the pressure, $\mathbf{g}$ is the gravitational acceleration, $T$ is the temperature, $\alpha_f$ is the thermal diffusivity, $\mathbf{F}$ are the external forces applied, $\rho_f$ and $\mu_f$ is the density and the viscosity of the fluid, respectively. In order to obtain a set of non-dimensional equations, we consider three different cases of convective heat transfer. Initially, we study the forced convection problem, followed by the natural and the mixed convection problems and, we obtain the non-dimensional form of the equations for each case.

*Forced convection*

In forced convection problems the following non-dimensional scales are usually employed:

$$x = \frac{x^*}{L}, \quad y = \frac{y^*}{L}, \quad u = \frac{u^*}{U}, \quad v = \frac{v^*}{U},$$

$$p = \frac{p^*}{\rho U^2}, \quad T = \frac{T^* - T_a}{T_H - T_a}, \tag{18}$$

where $L$ is a characteristic dimension, the subscript $\alpha$ indicates a constant reference value of temperature and $T_H$ is a constant reference temperature. Substituting of the above form into the dimensional formulation and taking the curl of the equation, we obtain the non-dimensional form of the equations in velocity-vorticity formulation:

$$\nabla^2 u = -\frac{\partial \omega}{\partial y}, \tag{19}$$

$$\nabla^2 v = \frac{\partial \omega}{\partial x}, \tag{20}$$

$$u\frac{\partial \omega}{\partial x} + v\frac{\partial \omega}{\partial y} = \frac{1}{Re}\left(\frac{\partial^2 \omega}{\partial x^2} + \frac{\partial^2 \omega}{\partial y^2}\right), \tag{21}$$

$$u\frac{\partial T}{\partial x} + v\frac{\partial T}{\partial y} = \frac{1}{Re\,\mathrm{Pr}}\left(\frac{\partial^2 T}{\partial x^2} + \frac{\partial^2 T}{\partial y^2}\right), \tag{22}$$

where $Re = \frac{\rho_f UL}{\mu_f}$ and $Pr = \frac{\mu_f}{\alpha_f \rho_f}$ are the Reynolds and the Prandtl numbers, respectively, while $U$ and $L$ are the maximum velocity and the characteristic length.

### *3.1.1 Natural or Buoyancy-driven convection*

Natural convection is generated by the density difference induced by the temperature differences within the fluid. In most buoyancy-driven convection problems, flow is generated by either a temperature variation or a concentration variation in the fluid, which leads to local density differences. For temperature-driven flows and using the Boussinesq approximation, we can write

$$g\left(\rho - \rho_a\right) = g\beta\left(T - T_a\right),$$

where $g$ is the acceleration due to gravity and $\beta$ is the coefficient of thermal expansion. Using the following non-dimensional scales (e.g. Eq. 23) for natural convection, in the absence of a reference velocity value,

$$x = \frac{x^*}{D}, \quad y = \frac{y^*}{D}, \quad u = \frac{u^* D}{\alpha_f},$$

$$v = \frac{v^* D}{\alpha_f}, \quad p = \frac{p^* D^2}{\rho \alpha_f^2}, \quad T = \frac{T^* - T^*_{wc}}{T^*_{wh} - T^*_{wc}} \tag{23}$$

we get the equations in velocity-vorticity formulation:

$$\nabla^2 u = -\frac{\partial \omega}{\partial y}, \tag{24}$$

$$\nabla^2 v = \frac{\partial \omega}{\partial x}, \tag{25}$$

$$u\frac{\partial \omega}{\partial x} + v\frac{\partial \omega}{\partial y} = Pr\left(\frac{\partial^2 \omega}{\partial x^2} + \frac{\partial^2 \omega}{\partial y^2}\right) + RaPr\frac{\partial T}{\partial x}, \tag{26}$$

$$u\frac{\partial T}{\partial x} + v\frac{\partial T}{\partial y} = \frac{\partial^2 T}{\partial x^2} + \frac{\partial^2 T}{\partial y^2}, \tag{27}$$

where $Ra = \frac{g\rho_f \beta \Delta T D^3}{\mu_f a_f}$ is the Rayleigh number and $\Delta T = T^* - T^*_{wc}$.

### *3.1.2 Mixed convection*

Mixed convection involves both forced and natural flow conditions. The buoyancy effects become comparable to the forced flow effects at small and moderate Reynolds numbers. Thus, in mixed convection problems, the buoyancy term needs to be added to the appropriate component of the momentum equation. In mixed convection problems the following non-dimensional scales are usually employed:

$$x = \frac{x^*}{L}, \quad y = \frac{y^*}{L}, \quad u = \frac{u^*}{U}, \quad v = \frac{v^*}{U},$$

$$p = \frac{p^*}{\rho U^2}, \quad T = \frac{T^* - T_\alpha}{(T_H - T_\alpha)}. \tag{28}$$

Finally, we get:

$$\nabla^2 u = -\frac{\partial \omega}{\partial y}, \tag{29}$$

$$\nabla^2 v = \frac{\partial \omega}{\partial x}, \tag{30}$$

$$u\frac{\partial \omega}{\partial x} + v\frac{\partial \omega}{\partial y} = \frac{1}{Re}\left(\frac{\partial^2 \omega}{\partial x^2} + \frac{\partial^2 \omega}{\partial y^2}\right) + Ri\frac{\partial T}{\partial x}, \tag{31}$$

$$u\frac{\partial T}{\partial x} + v\frac{\partial T}{\partial y} = \frac{1}{RePr}\left(\frac{\partial^2 T}{\partial x^2} + \frac{\partial^2 T}{\partial y^2}\right), \tag{32}$$

where $Ri$ is the Richardson number defined as $Ri = \frac{Gr}{Re^2}$.

### 3.2 Solution Procedure

An iterative scheme is utilized for the solution of the velocity-vorticity formulation of the Navier-Stokes equations. In the majority of the incompressible flow problems modeled with Navier-Stokes equations the most natural boundary conditions arises when the velocity is prescribed all over the boundaries of the problem. The vorticity boundary conditions are determined iteratively from computations. The iterative solution algorithm used for the discretized fluid flow equations, must ensure coupled satisfaction of all the equations at convergence. We follow the approach of the so-called MAC algorithm proposed in [Harlow and Welch (1965)] and used in [Bourantas, Skouras, Loukopoulos and Nikiforidis (2010)]. More precisely, the process initiates from an initial velocity condition $\mathbf{u}^{(0)}$ that satisfies the continuity equation within the entire problem domain $\Omega(x,y)$, that is, $\nabla \cdot \mathbf{u}^{(0)} = 0$. Following, the velocity-Poisson equation is solved using the point collocation method by taking known vorticity components. A new velocity field $\mathbf{u}^{(*)}$ may be estimated from the velocity-Poisson equations. Finally, a simple point collocation procedure is applied. Collocation method is a special case of the weighted residual method, where the test function used is the Dirac delta function.

## 4 Numerical results

### 4.1 Forced convection in a square cavity

Forced convection problem in the square cavity (Fig. 1) was solved initially. By this, the energy equation is decoupled from the vorticity transport and velocity equations. The term conjugate heat transfer (CHT) is often associated with such a problem. In this case the driving force of the fluid motion is the top wall that slides with constant velocity. For the forced convection in the square cavity, results were obtained for the Reynolds number ranging from $Re = 400$ to $Re = 10000$. Constant fluid properties with the Prandtl number value of $Pr = 0.71$ were used for all cases. A $81 \times 81$ uniform mesh was employed for the Reynolds numbers $Re$ up to 400 and the number of the grid points increased up to $161 \times 161$ for $Re$ beyond that value in order to obtain grid independent results with the uniform mesh system.

Figure 2 shows the $u$ velocity distributions at the cavity vertical mid-plane $(x = 0.5)$ and $v$ profiles at the horizontal mid-plane $(y = 0.5)$ for Reynolds $Re = 400$, 1000, 5000 and 10000. This so-called lid-driven cavity flow is a well established benchmark problem and, the results were compared with those obtained in [Ghia, Ghia and Shin (1982):] and [Bourantas, Skouras, Loukopoulos and Nikiforidis (2010)]. In Fig. 3 the streamfunction and the temperature contours for Reynolds numbers from $Re = 400$ up to $Re = 10000$ are shown.

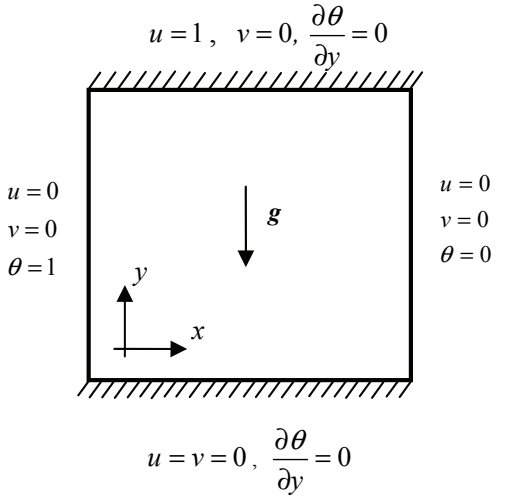


Figure 1: Geometry and the given boundary conditions for a square cavity.

### *4.2 Natural convection in a square cavity*

Flow in a square cavity is a well established and popular benchmark problem for testing a numerical scheme. The disadvantage of the driven cavity problem is that the moving lid introduces singularities at two of the corners. Thus, a more realistic benchmark problem was devised and introduced in [Davis, Jones and Roache (1979)], where the natural convection of a Boussinesq material in an enclosed cavity is induced by an imposed wall temperature difference. In this problem, the geometric simplicity of the driven cavity is maintained while the singularities are removed. Fluid flow is considered in a square cavity with insulated top and bottom walls and the side walls maintained at constant but different temperature (see Fig. 4).

A benchmark solution for this problem has been published [Davis, Jones and Roache (1979)]. The authors used a streamfunction-vorticity Finite Difference (FD) method with grids up to 81 x 81 points, and employed Richardson extrapolation to obtain more accurate benchmark solutions for Rayleigh numbers ($Ra$) up to $10^6$. The top wall was considered to be stationary and the fluid motion is caused solely by the buoyancy effects. Applying the meshless point collocation scheme with LRBF interpolation the Rayleigh number $Ra = GrPr$ was varied from $10^2$ to $10^6$ and a constant Prandtl number of 0.72 was used. A $81 \times 81$ uniform mesh was employed for the Reynolds numbers $Re$ up to 400 and the number of the grid points increased up to $121 \times 121$ for $Re$ beyond that value in order to obtain grid independent results

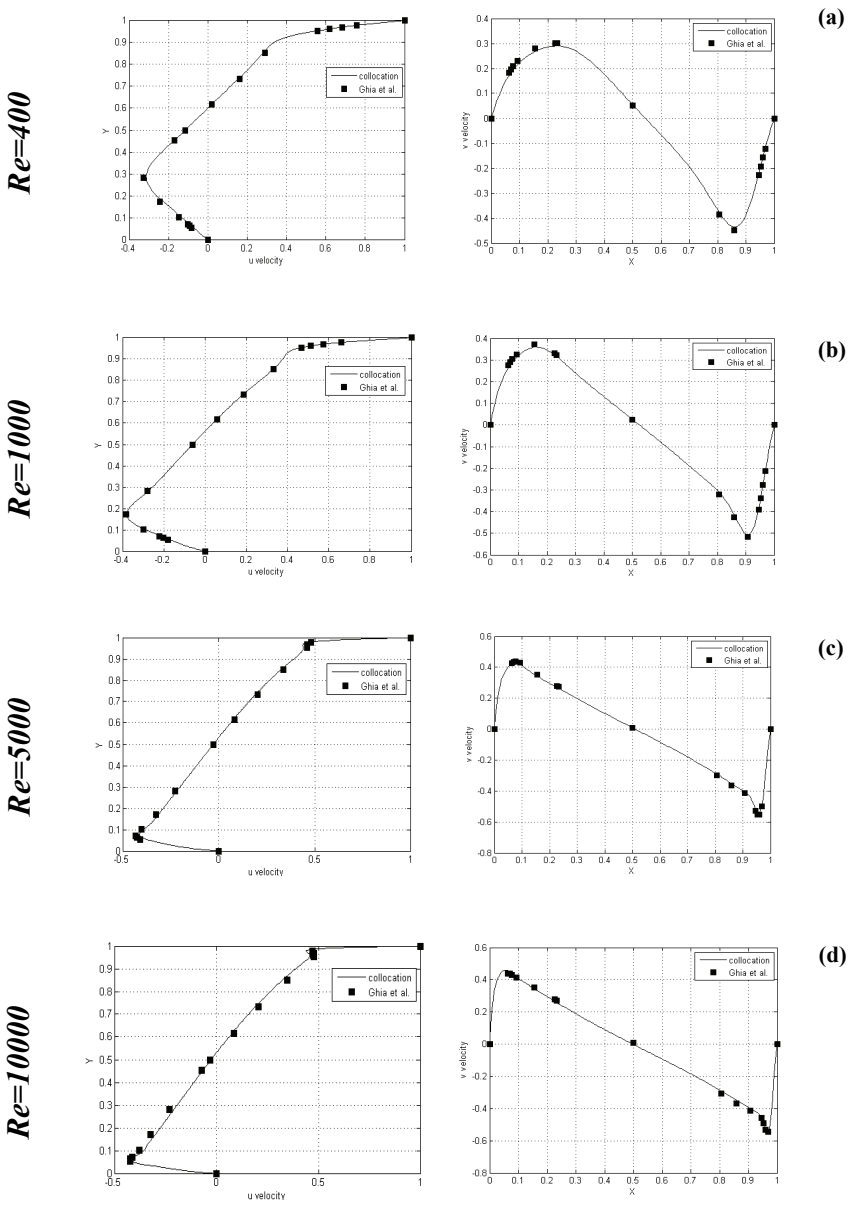


Figure 2: The $u$-velocity on the vertical section $x = 0.5$ and the $v$-velocity on the horizontal section $y = 0.5$ of the square lid-driven cavity problem for **(a)** $Re = 400$ **(b)** $Re = 1000$ **(c)** $Re = 5000$ and **(d)** $Re = 10000$. Results of [Ghia *et. a.l.*, 1982] are compared with the current numerical solutions.

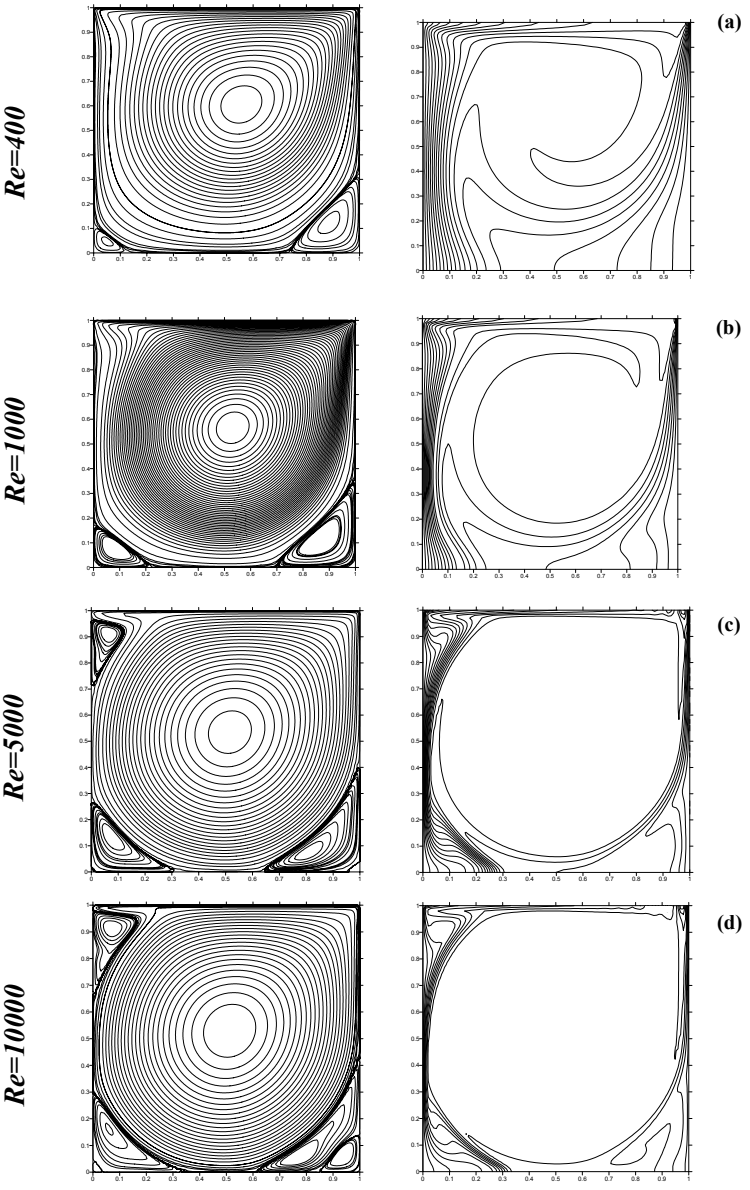


Figure 3: The streamfunction and the isotherms contour plots of the square lid-driven cavity problem for **(a)** $Re = 400$ **(b)** $Re = 1000$ **(c)** $Re = 5000$ and **(d)** $Re = 10000$. Results of [Ghia *et. a.l.*, 1982] are compared with the current numerical solutions.

with the uniform mesh system. In general, the agreements of the present solution obtained by the velocity-vorticity formulation with those given in [Davis, Jones and Roache (1979)] are excellent.

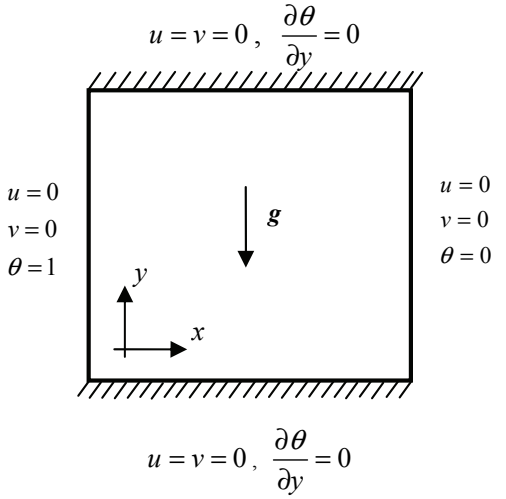


Figure 4: Configuration of natural convection in a square cavity.

In the present problem the convergence criterion is set at $10^{-6}$. In order to chech the performance of local type meshless point collocation with LRBF interpolation, the following quantities were computed as in [Shu, Ding and Yeo (2003)]:

$|\psi_{mid}|$ the stream function at the mid-point of the cavity,

$|\psi_{\max}|$ the maximum absolute value of the stream function,

$u_{\max}$ the maximum horizontal velocity on the vertical mid-plane of the cavity,

$v_{\max}$ the maximum vertical velocity on the horizontal mid-plane of the cavity,

$N_{u_0}$ the average Nusselt number on the vertical boundary of the cavity at $x = 0$ defined by

$Nu_0 = Nu|_{x=0}$ where $Nu_1(\mathbf{x}) = \int_0^1 (u_1 T - T_{,1}) dy$,

$N_{u_{\max}}$ the maximum value of the local Nusselt number on the boundary at $x = 0$,

$N_{u_{\min}}$ the minimum value of the local Nusselt number on the boundary at $x = 0$.

The numerical results obtained here are compared with the benchmark Finite Difference numerical solution [Davis (1979)] and the Indirect Radial Basis Functions Networks (IRBFN) [Dui and Tran-Kong (2001)]. Tables 2-5 list the numerical

results achieved by different numerical methods for Rayleigh numbers of $10^3$, $10^4$, $10^5$ and $10^6$, respectively. The isotherms and streamlines of $Ra = 10^3$ up to $Ra = 10^6$, are shown in Fig. 5. It can be observed that for all the Rayleigh numbers, the numerical results of the meshless point collocation method agree very well with the benchmark solution.

Figure 5 demonstrates that a single circulation cell is formed in the clockwise direction for all values of Rayleigh numbers. As the Rayleigh number increases, the length cell increases and egg shaped cell is observed as shown in Figure 5b. With even more increasing of the value of Rayleigh number the flow strength increases and the boundary layers become more distinguished. Isotherms show that temperature gradients near the heater and cold wall become more severe. For $Ra = 10^5$, the streamlines elongate parallel to the horizontal wall.

### *4.3 Mixed convection in a square cavity*

Following, mixed convection flow and temperature fields in a lid-driven square cavity are examined and the numerical results are compared with those obtained in [Aydin (1999)]. The dimensional parameter that characterizes the flow is the Richardson $(Ri)$ number. From the physical point of view, $Ri$ characterizes the relative importance of buoyancy to forced convection. More precisely, for $Ri < 1$, the flow and heat transfer is dominated by forced convection, while for $Ri > 1$, it is dominated by natural convection. Finally, when $Ri = 1$, the flow is a mixed regime.

The physical model under consideration is in Fig. 6. The left wall is moving across the cavity from bottom to top at a constant velocity. Furthermore, the flow is considered to be two-dimensional, steady and laminar. Both upper and lower walls were considered adiabatic, while the left and the right walls are the hot and the cold, respectively (Fig. 6a), or vice versa (Fig. 6b). The Richardson number $(Ri)$ is varied from 0.01 to 100.0 in order to simulate forced convection, pure mixed convection and free convection dominated flow in the cavity.

From the physical point of view, the two different thermal boundary conditions used, result in two different heat transfer mechanisms, namely buoyancy aiding and buoyancy opposing. For the buoyancy aiding case, where the hot left and the cold right walls were considered, the resulting buoyancy induce a clockwise rotating flow. In this flow, cell recirculation is enforced, driven by the moving left wall, while the buoyancy has an adding result on the forced convection flow. For the buoyancy opposing case, for the cold left and the hot right walls, the buoyancy tends to induce a counter-clockwise flow, opposed to the lid-driven recirculation.

In Figs. 7 and 8 the streamlines (left) and the isotherms (right) are presented at various values of mixed convection parameter $Ri$, for the buoyancy aiding and buoy-

Table 2: Numerical result for natural convection in a square cavity for $Ra = 10^3$.

| **Parameters** | $Ra = 10^3$ | | | | | |
|---|---|---|---|---|---|---|
| | **MPC (LRBF-GA)** | **LRBF-DQ** | **Mai-Duy *et al.*** | **Wu *et al.*** | **Sarler** | **Davis** |
| $\lvert\psi_{mid}\rvert$ | 1.174 | N/A | N/A | N/A | 1.170 | 1.174 |
| $\lvert\psi_{\max}\rvert$ | 1.174 | N/A | N/A | 1.175 | N/A | 1.174 |
| $u_{\max}$ | 3.649 | N/A | 3.651 | 3.634 | 3.633 | 3.649 |
| $v_{\max}$ | 3.696 | N/A | 3.699 | 3.687 | 3.680 | 3.697 |
| $N_{u_0}$ | 1.119 | N/A | 1.18 | N/A | 1.118 | 1.118 |
| $N_u^{\max}$ | 1.506 | N/A | N/A | 1.507 | N/A | 1.505 |
| $N_u^{\min}$ | 0.691 | N/A | N/A | 0.692 | N/A | 0.692 |

Table 3: Numerical result for natural convection in a square cavity for $Ra = 10^4$.

| **Parameters** | $Ra = 10^4$ | | | | | |
|---|---|---|---|---|---|---|
| | **MPC (LRBF-GA)** | **LRBF-DQ** | **Mai-Duy *et al.*** | **Wu *et al.*** | **Sarler** | **Davis** |
| $\lvert\psi_{mid}\rvert$ | 5.082 | 5.084 | N/A | N/A | 4.955 | 5.071 |
| $\lvert\psi_{\max}\rvert$ | 5.082 | N/A | N/A | 5.065 | N/A | 5.071 |
| $u_{\max}$ | 16.176 | 16.169 | 16.195 | 16.148 | 16.09 | 16.178 |
| $v_{\max}$ | 19.620 | 19.631 | 19.197 | 19.694 | 19.59 | 19.617 |
| $N_{u_0}$ | 2.238 | 2.240 | 2.238 | N/A | 2.246 | 2.238 |
| $N_u^{\max}$ | 3.530 | 3.560 | N/A | 3.547 | N/A | 3.528 |
| $N_u^{\min}$ | 0.584 | 0.584 | N/A | 0.587 | N/A | 0.586 |

Table 4: Numerical result for natural convection in a square cavity for $Ra = 10^5$.

| **Parameters** | $Ra = 10^5$ | | | | | |
|---|---|---|---|---|---|---|
| | **MPC (LRBF-GA)** | **LRBF-DQ** | **Mai-Duy *et al.*** | **Wu *et al.*** | **Sarler** | **Davis** |
| $\lvert\psi_{mid}\rvert$ | 9.121 | 9.146 | N/A | N/A | 9.073 | 9.111 |
| $\lvert\psi_{\max}\rvert$ | 9.642 | 9.648 | N/A | 9.766 | N/A | 9.612 |
| $u_{\max}$ | 34.830 | 34.547 | 34.790 | 35.243 | 34.08 | 34.730 |
| $v_{\max}$ | 68.690 | 69.313 | 68.694 | 69.447 | 68.27 | 68.590 |
| $N_{u_0}$ | 4.519 | 4.573 | 4.583 | N/A | 4.523 | 4.519 |
| $N_u^{\max}$ | 7.717 | 7.844 | N/A | 9.197 | N/A | 7.717 |
| $N_u^{\min}$ | 0.729 | 0.726 | N/A | 0.729 | N/A | 0.729 |

Table 5: Numerical result for natural convection in a square cavity for $Ra = 10^6$.

| **Parameters** | $Ra = 10^6$ | | | | | |
|---|---|---|---|---|---|---|
| | **MPC (LRBF-GA)** | **LRBF-DQ** | **Mai-Duy *et al.*** | **Wu *et al.*** | **Sarler** | **Davis** |
| $\lvert\psi_{mid}\rvert$ | 16.320 | 16.505 | N/A | N/A | 16.22 | 16.320 |
| $\lvert\psi_{\max}\rvert$ | 16.750 | 16.863 | N/A | N/A | N/A | 16.750 |
| $u_{\max}$ | 64.630 | 64.362 | 64.65 | N/A | 63.12 | 64.630 |
| $v_{\max}$ | 219.36 | 222.10 | 220.29 | N/A | 215.56 | 219.36 |
| $N_{u_0}$ | 8.817 | 8.932 | 9.273 | N/A | 8.834 | 8.817 |
| $N_u^{\max}$ | 17.925 | 18.390 | N/A | N/A | N/A | 17.925 |
| $N_u^{\min}$ | 0.989 | 0.975 | N/A | N/A | N/A | 0.989 |

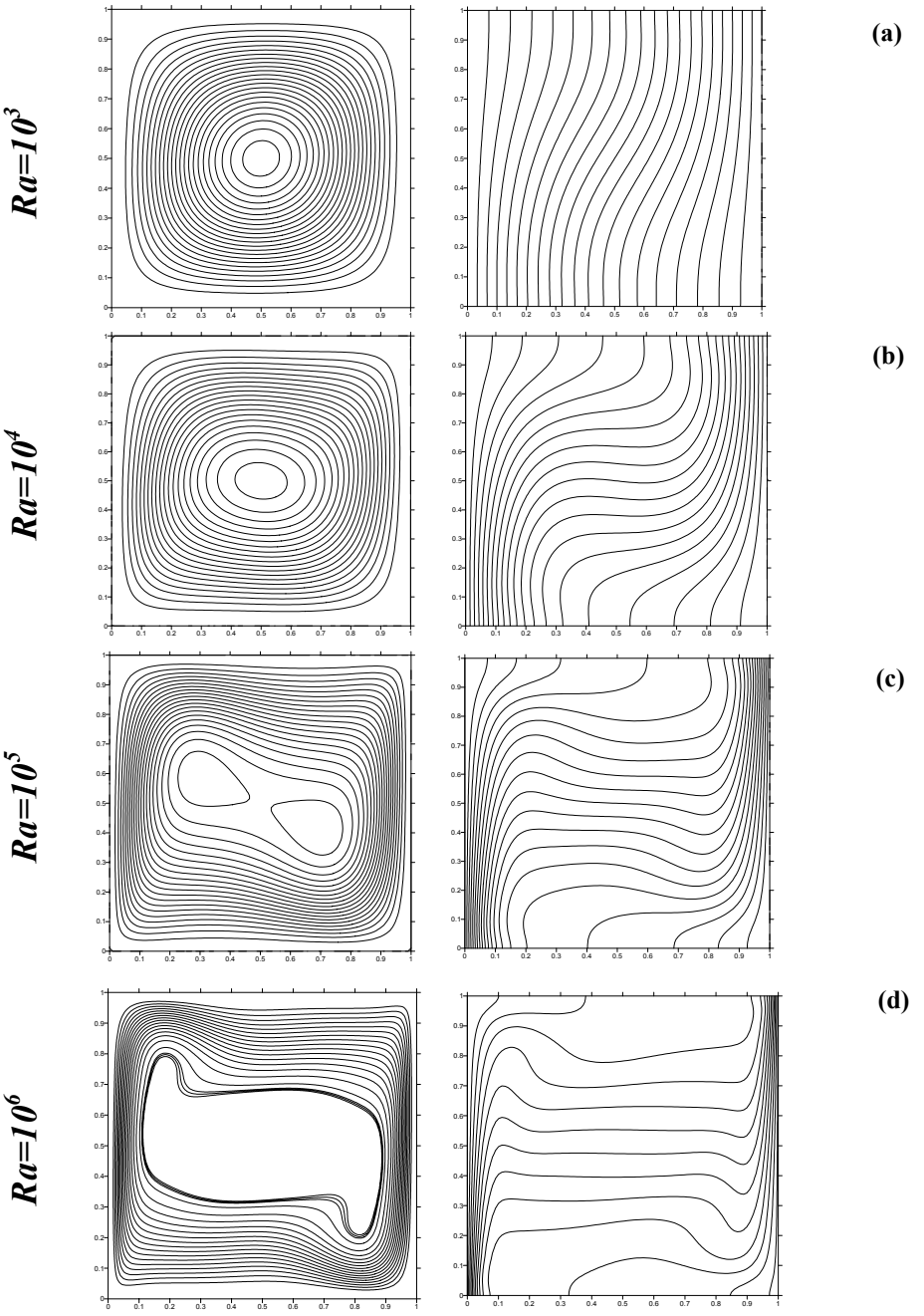


Figure 5: Streamlines and isotherms of **(a)** $Ra = 10^3$ **(b)** $Ra = 10^4$ **(c)** $Ra = 10^5$ and **(d)** $Ra = 10^6$.

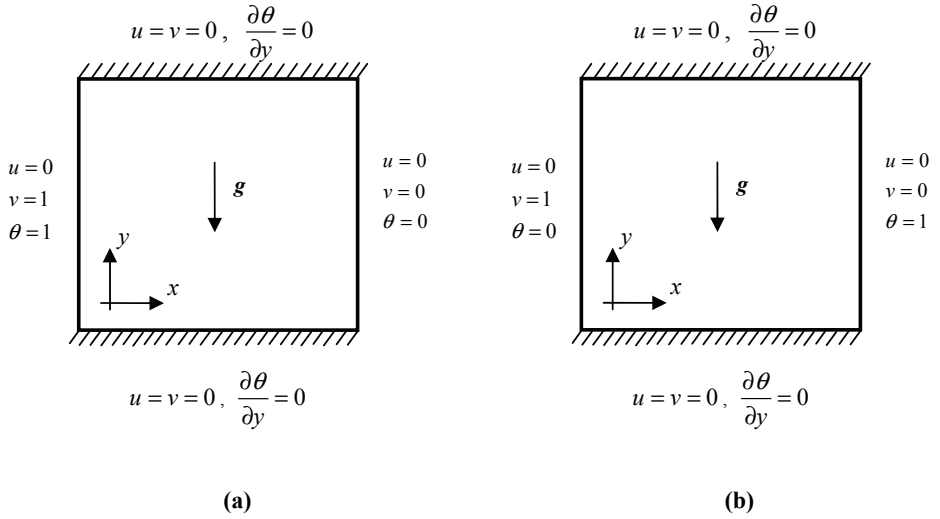


Figure 6: Geometry configuration and boundary conditions for mixed convection.

ancy opposing flows, respectively. The Reynolds number $Re$ was kept constant at $Re = 100$. In every case seven different values of Richardson $(Ri)$ number were used namely, 0.01, 0.1, 0.5, 1, 2, 10 and 100.

In details, as it can be seen from the Fig. 7, for the case of buoyancy aiding flow, an increase of $Ri$ from 0.01 to 0.1 does not change significantly the flow and temperature fields. In this case, the forced convection remains dominant over the natural convection, because the buoyancy is still weak to affect the flow pattern. When the $Ri$ increases from 0.1 to 0.5 the strength of the cell is enhanced and the isotherms tend to be stratified, due to the effect of the buoyancy on the flow and the temperature field. When $0.5 < Ri < 2$, the buoyancy and shear effects are comparable. As $Ri$ approach 0.5 and 2.0, it makes the shear and buoyancy effect important, respectively. For $Ri$ 10 and 100, the flow and the temperature fields are almost the same as those in natural convection, indicating that the natural convection is the dominant mechanism over the forced convection.

As far as the opposing buoyancy, as it can be observed at Fig. 8, there is no significant difference in streamlines and isotherms for $Ri = 0.01$ and 0.1. When $Ri$ is increased beyond 0.1, the cellular motion is destroyed, leading to a new flow type. When, $Ri = 0.5$ a secondary cell is generated due to buoyancy effects. This secondary cell is counter-rotating with respect to the original cell due to the motion of the left wall. With the increasing value of Richardson number this secondary cell, originating from the buoyancy, becomes larger due to the shear, restricting the

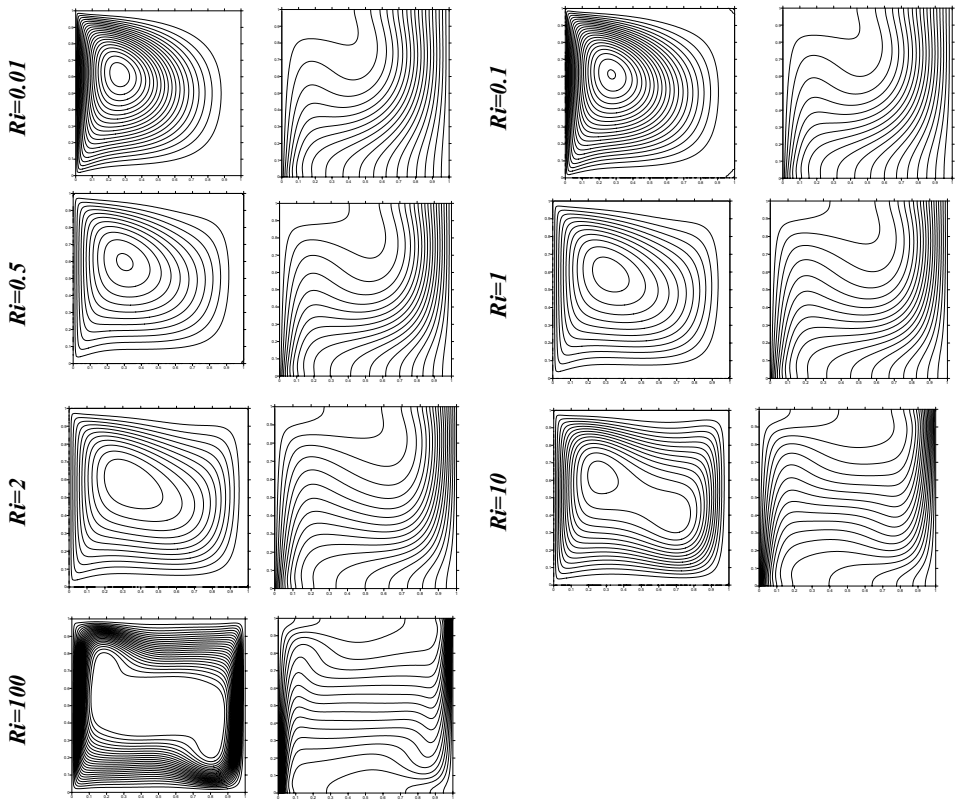


Figure 7: The streamlines (left) and the isotherms (right) at different values of Richardson ($Ri$) number for aiding buoyancy.

primary cell to a region adjacent to the left vertical wall. At $Ri = 10$, the forced convection cell becomes restricted to a very small region. Finally, when $Ri = 100$, the primary cell is disappeared and the flow field is dominated by the buoyancy. All results are qualitatively compared with corresponding presented in [Aydin (1999)] and the agreement is obvious.

## 5 Conclusions

A meshless, point collocation with Local Radial Basis Functions (LRBF) interpolation based method is presented for the numerical solution of the incompressible, non-isothermal Navier-stokes equations in velocity-vorticity formulation. A velocity-correction method is applied ensuring the continuity equation. The numerical results were compared with the solution of benchmark problems. From

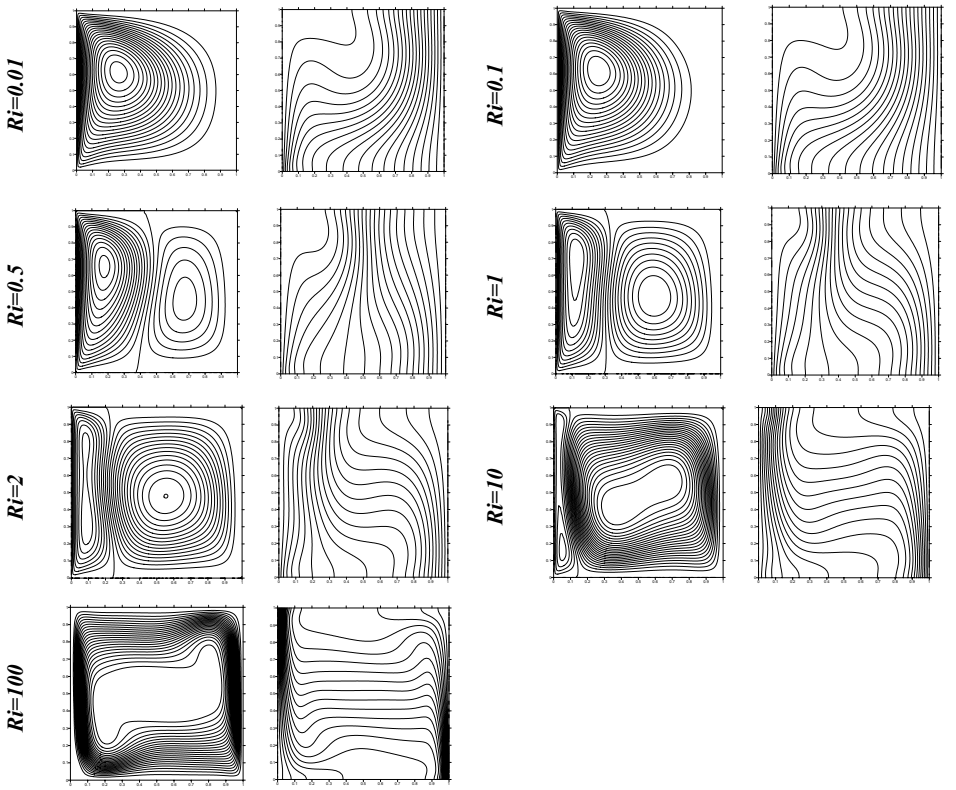


Figure 8: The streamlines (left) and the isotherms (right) at different values of Richardson $(Ri)$ number for opposing buoyancy.

the comparison made, it can be seen that the presented method can solve incompressible, non-isothermal, viscous flow problems accurately. As benchmark problems the forced, natural and mixed convection in a rectangular domain were studied. In every case, solutions were obtained for high values of the characteristics non-dimensional numbers of the flow, that is, the Reynolds, the Rayleigh and the Richardson number. The numerical scheme is accurate and efficient, yet for relatively coarse grids.

All the above computations were taken place using a uniform $161 \times 161$ grid. Furthermore, the choice of the specific nodal configuration was taken after a grid independence study. For that reason we used grids of $81 \times 81$, $121 \times 121$ and $161 \times 161$ nodes. A shape parameter $c = 3$ and the nine close neighbors as the support domain were used. The condition number was calculated as $6.482 \times 10^{13}$. It is important to notice that the proposed meshless numerical scheme can be applied in cases were

irregular geometries are present. Also, the nodal distributions can be regular or irregular, but it requires a trial and error procedure for the determination of both, the suitable nodal distribution and the shape parameter c, so that the condition number takes high values.

**Acknowledgement:** Work was supported by the program "K. Karatheodoris 2008" - Funding of research group in University of Patras, Greece, with P.C.: C.596.

## References

**Arefmanesh, A.; Najafi, M.; Abdi, H.** (2008): Meshless local Petrov-Galerkin method with unity test function for non-isothermal fluid flow. *CMES: Computer Modeling in Engineering and Sciences*, vol. 25, pp. 9-22.

**Atluri, S. N.; Shen, S.P.** (2002): *The Meshless Local Petrov–Galerkin (MLPG) Method*, 440 pages, Tech Science Press, Encino USA.

**Aydin, O.** (1999): Aiding and opposing mechanisms of mixed convection in a shear and buoyancy-driven cavity. *International Communications in Heat and Mass Transfer*, vol. 26, pp. 1019-1028.

**Belytschko, T.; Krongauz, Y.; Organ D.; Fleming, M.; Krysl, P.** (1996): Meshless methods: an overview and recent developments. *Computer Methods in Applied Mechanics and Engineering*, vol. 139, pp. 3-47.

**Bourantas, G. C.; Skouras, E. D.; Loukopoulos, V. C.; Nikiforidis, G. C**. (2010): Meshfree point collocation schemes for 2D steady state incompressible Navier-Stokes equations in velocity-vorticity formulation for high values of Reynolds numbers. *CMES: Computer Modeling in Engineering and Sciences*, vol. 1451, pp. 1-33.

**Chen, W.** (2002): New RBF collocation schemes and kernel RBFs with applications. *Lecture Notes in Computational Science and Engineering*, vol. 26, pp. 75-86.

**Chen, C.S.; Ganesh, M.; Golberg, M.A.; Cheng A.H.D**. (2002): Multilevel compact radial basis functions based computational scheme for some elliptic problems, *Computers & Mathematics with Applications*, vol. 43, pp. 359-378.

**Ghia, U.; Ghia, K. N.; Shin, C. T.** (1982): High-Re solutions for incompressible flow using the Navier-Stokes equations and a multigrid method. *Journal of Computational Physics*, vol. 48, pp. 387-411.

**De Vahl Davis, G.; Jones. I,P.; Roache P.J.** (1979): Natural convection in an enclosed cavity: a comparison problem. *Computers and Fluids,* vol.7, pp. 315–

316.

**Divo, E.; Kassab, A.** (2006): Iterative domain decomposition meshless method modeling of incompressible viscous flows and conjugate heat transfer. *Engineering Analysis with Boundary Elements*, vol. 30, pp. 465–478.

**Divo E.; Kassab A.** (2007): An efficient localized RBF meshless method for fluid flow and conjugate heat transfer. *ASME Journal of Heat Transfer* , vol. 129, pp. 124–36.

**Divo E.; Kassab A.** (2008): Localized meshless modeling of natural convective viscous flows. *Numerical Heat Transfer, Part B: Fundamentals*, vol. 53, pp. 487–509.

**Fasshauer, G.** (1997): Solving partial differential equations by collocation with radial basis functions. In Surface Fitting and Multiresolution Methods. Edited by A.L. Mehaute, C. Rabut and L.L. Schumaker.

**Fasshauer, G,** (2007): Meshfree Approximation Methods with MATLAB, World Scientific.

**Ho-Minh, D.; Mai-Duy, N.; Tran-Cong, T.** (2009): A Galerkin-RBF approach for the streamfunction-vorticity-temperature formulation of natural convection in 2D enclosured domains. *CMES: Computer Modeling in Engineering and Sciences*, vol. 44, pp. 219-248.

**Harlow, F. H.; Welch, J. E.** (1965): Numerical calculation of time dependent viscous incompressible flow of fluids with a free surface. *Physics of Fluids*, vol. 8, pp. 2182–2189.

**Kansa, E.J.** (1990): Multiquadrics scattered data approximation scheme with applications to computational fluid-dynamics. I. Surface approximations and partial derivative estimates. *Applied Mathematics and Computation*, vol. 19, pp. 127–145.

**Kosec, G.; Sarler, B.** (2008): Solution of thermal-fluid problems by collocation with local pressure correction. *International Journal of Numerical Methods for Heat & Fluid Flow*, vol. 18, pp. 868-882.

**Lee, C.K.; Liu, X.; Fan, S.C.** (2003): Local multiquadric approximation for solving boundary value problems, *Computational Mechanics, v*ol. 30, pp. 396-409.

**Liu, G. R**. (2002): *Mesh Free Methods, Moving beyond the Finite Element Method*, CRC Press.

**Liu, G. R,; Gu Y. T,** (2005): *An introduction to meshfree methods and their programming*. Springer, The Netherlands.

**Mai-Duy, N.; Tran-Cong, T.** (2001): Numerical solution of Navier-Stokes equations using multiquadric radial basis function networks. *International Journal for Numerical Methods in Fluids*,vol. 37, pp. 65-86.

**Mai-Duy, N.; Tran-Cong, T.** (2002): Mesh-free radial basis function network methods with domain decomposition for approximation of functions and numerical solution of Poisson's equations, *Engineering Analysis with Boundary Elements*, vol. 26, pp. 133-156.

**Mai-Duy, N.; Tran-Cong, T.** (2003): Indirect RBPN method with thin plate splines for numerical solution of differential equations. *CMES: Computer Modeling in Engineering and Sciences*, vol. 4, pp. 85-102.

**Power, H.; Barraco, W.A.** (2002): Comparison analysis between unsymmetric and symmetric RBFCMs for the numerical solution of PDEs. *Computers and Mathematics wit Applications,* vol. 43, pp. 551-583.

**Power, H.; Barraco, V.** (2002): A comparison analysis between unsymmetric and symmetric radial basis function collocation methods for the numerical solution of partial differential equations. *Computers and Mathematics with Applications*, vol. 43, pp. 551-583.

**Roache, P.J.** (1998): *Verification and Validation in Computational Science and Engineering*. Hermosa Publishers: Albuquerque, NM, 1998.

**Sarler, B.** (2005): A radial basis function collocation approach in Computational Fluid dynamics. media. *CMES: Computer Modeling in Engineering and Sciences*, vol. 7, pp. 185-193.

**Sarler, B.; Perko, J.; Chen, C.S.** (2004): Radial basis function collocation method solution of natural convection in porous media. *International Journal of Numerical Methods for Heat & Fluid Flow*, vol. 14, pp.187–212.

**Sarler, B.; Vertnik, R.** (2006): Local explicit radial basis function collocation method for diffusion problems. *Computers and Mathematics with Applications*, vol. 51, pp. 1269–82.

**Shu, C.; Ding, H.; Yeo K.S.** (2003): Local radial basis function-based differential quadrature method and its application to solve two-dimensional incompressible Navier–Stokes equations. *Computer Methods in Applied Mechanics and Engineering*, vol. 192, pp. 941–954.

**Wu, Y.L.; Liu, G.R.** (2003): A meshfree formulation of local radial point interpolation method (LRPIM) for incompressible flow simulation, *Computational Mechanics*, vol. 30, pp. 355-365.